Circularly polarized light emission in scanning tunneling microscopy of magnetic systems

S. P. Apell
Department of Applied Physics, Chalmers University of Technology and Göteborg University, S-412 96 Göteborg, Sweden

D. R. Penn
Electron Physics Group, National Institute of Standards and Technology, Gaithersburg, Maryland 20899

P. Johansson
Department of Theoretical Physics, University of Lund, Sölvegatan 14 A, S-223 62 Lund, Sweden
(Received 28 April 1999)

Light is produced when a scanning tunneling microscope is used to probe a metal surface. Recent experiments on cobalt utilizing a tungsten tip found that the light is circularly polarized; the sense of circular polarization depends on the direction of the sample magnetization, and the degree of polarization is of order 10%. This raises the possibility of constructing a magnetic microscope with very good spatial resolution. We present a theory of this effect for iron and cobalt and find a degree of polarization of order 0.1%. This is in disagreement with the experiments on cobalt as well as previous theoretical work which found order of magnitude agreement with the experimental results. However, a recent experiment on iron showed $0.0 \pm 2\%$. We predict that the use of a silver tip would increase the degree of circular polarization for a range of photon energies.

I. INTRODUCTION

The last ten years have seen a rapid development of the field of magnetic dichroism, especially where the response of a system to left and right circularly polarized light is probed; so called circular dichroism.[1] For a magnetic material this is magnetic circular dichroism (MCD). Experiments involve x-ray absorption,[2] as well as standard photoemission techniques.[3]

The possibility of a method of microscopic measurements of surface magnetism has been suggested by a recent experiment.[4] In this experiment, circularly polarized light emitted from a scanning tunneling microscope (STM) was observed when the surface of a ferromagnetic material (Co) was probed with a W tip in a longitudinal configuration (see Fig. 1, the applied magnetic field is parallel to both the surface plane and to the plane of light detection). The handedness of the circular polarization was found to depend on the direction of the applied field and the degree of polarization was between 5 and 10 %. The results of Vázques de Parga and Alvarado[4] looks, at first sight, to have been corroborated by the theoretical work of Majlis *et al.*[5] In principle such an effect, if confirmed, should make it possible to map the magnetic microstructure of a surface by measuring the circular polarization of the emitted light while scanning the surface because a STM tip provides very good spatial resolution.[6] However, a more recent experiment of this type, by Pierce *et al.*[7] carried out on Fe with a W tip, found $0.0 \pm 2\%$ circular polarization.

In this paper we calculate the degree of circular polarization for Fe and Co. We find two contributions to the circular polarization. The first is due to the Kerr rotation of the light emitted in the tunneling process. The second contribution is due to the polarization of the scanning tip by the electric field of the emitted light. The polarized tip radiates and the radiation undergoes a Kerr rotation. This second contribution depends on the polarizability of the tip as well as the dielectric properties of the sample and can be significantly larger than the first contribution.

We obtain results which are between one and two orders of magnitude smaller than that measured by Vázques de Parga and Alvarado[4] but consistent with the measurements of Pierce *et al.*[7] Both workers used W tips, but we find that for a Ag tip, Co and Fe produce a larger degree of circular polarization for a range of photon energies.

There are other sources of circular polarization that are not magnetic in origin. For example, experiments by Vázques de Parga and Alvarado[8] and theory by Anisimovas

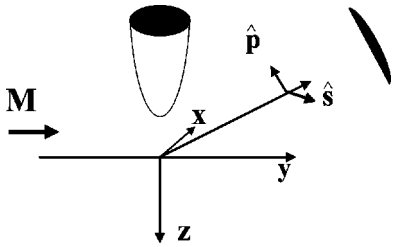

FIG. 1. The schematic experimental set-up in the experiments of Vázques de Parga and Alvarado (Ref. 4) and Pierce *et al.* (Ref. 7) showing the relative orientation of the applied magnetic field (**M**) in the plane of the Co(0001)/Fe(001) surface (x,y plane), tungsten tip orientation, and optical detection axis. With the help of the so called reciprocity theorem [Eq. (4)] one can relate the field intensity at the detector due to a current at the tip [E^T (detector)] to the ''detector-generated'' field intensity between tip and sample (E^D). The latter is easier to construct and hence makes it rather straightforward to find the field we are most interested in; the one in the tip region. $\hat{\mathbf{s}}$ ($=\hat{\mathbf{x}}$) and $\hat{\mathbf{p}}$ denote two orthogonal polarization directions at the detector.

and Johansson[9] show that an asymmetric STM tip can produce a degree of circular polarization on the order of 10%.

In Sec. II we develop a theory for the degree of circular polarization produced by an STM tip in the presence of a magnetic sample based on the magneto-optic Kerr effect. In order to understand the physics of the magnetic circular dichroism in these experiments the tip is modeled by a dipole. The purpose of the dipole model is solely to help to understand the physics and is introduced mainly for pedagogical reasons. In Sec. III the theoretical description of the tip is improved for the purpose of obtaining reliable numerical estimates of the degree of circular polarization. These results are discussed in Sec. IV.

II. THEORY

In this section we obtain an expression for the circular polarization of light emitted when an STM tip scans a magnetic material. The calculation is divided into five parts. (A) We first describe the experiment and express the results in terms of Stokes parameters. (B) The electromagnetic fields in the tip region are related to the fields at the detector. (C) A model for the tip is introduced which makes the problem tractable. (D) The local field outside the tip is related to the tip polarization, in the presence of a magnetic substrate. (E) The different contributions are assembled and we obtain a theoretical expression for the changes in the circular polarization due to a change in the direction of the applied magnetic field.

A. Theoretical expression for MCD

In this section we relate the MCD to the field amplitudes at the detector. The experiments by Vázques de Parga and Alvarado[4] and Pierce *et al.*[7] used the longitudinal configuration, i.e., the applied magnetic field is parallel to the plane of incidence and in the surface plane of Co(0001) [thin film grown on Au(111)] and Fe(001) (whisker), respectively. Light was detected at an angle of 30° measured from the surface and tungsten tips were used in both experiments. The emitted radiation showed circular polarization which changed when the applied magnetic field was reversed. Whereas Vázques de Parga and Alvarado[4] used a fixed quarter wave plate and carry out the analysis by a linear polarizer, Pierce *et al.*[7] use a rotating quarter wave plate and a fixed linear analyzer. In both experiments control measurements were performed on clean Au(111) samples and yielded no change of the polarization of the emitted light upon *reversal* of the external magnetic field. The background due to geometric details of tip-sample junctions such as those discussed in Refs. 8 and 9 and any residual dichroism of the view port of the UHV system were removed by reversing the magnetization of the sample.

The results of the two groups were very different. Pierce *et al.*[7] found no magnetization dependent circular polarization within an experimental uncertainty of $\pm 2\%$ whereas Vázques de Parga and Alvarado[4] found values of the order 5–10 %. An earlier experiment using a Ni tip, thus injecting spin-polarized electrons, and a Ni polycrystal sample also showed a large MCD upon reversal of the magnetization of the tip.[10]

Expressing the degree of polarization $\rho^{\pm}$ of the emitted light in terms of Stoke's parameters we have

$$\rho^{+}-\rho^{-}=\frac{S_3^{+}-S_3^{-}}{S_0}. \tag{1}$$

The superscripts on S_3 and ρ indicate whether the magnetization is parallel $(+)$ or antiparallel $(-)$ to the surface projection $\mathbf{k}$, of the photon wave vector. Following the definition given by Jackson[11] and concentrating on ρ^{+}, left-circular polarized light (positive helicity) has the polarization vector $\hat{\epsilon}_{+}=(\hat{p}-i\hat{s})/\sqrt{2}$, whereas for right-circular polarization $\hat{\epsilon}_{-}=(\hat{p}+i\hat{s})/\sqrt{2}$, where, see Fig. 1, $\hat{s}=\hat{x}$ and $\hat{p}=\hat{\theta}$ are *s*- and *p*-polarization unit vectors. In terms of the electric field $\mathbf{E}_{s,p}^{\mathrm{T}}$ at the detector caused by the source at the tip (T), the Stokes parameters are

$$S_0\equiv|\hat{\epsilon}_{+}^{*}\cdot\mathbf{E}_{s,p}^{\mathrm{T}}|^2+|\hat{\epsilon}_{-}^{*}\cdot\mathbf{E}_{s,p}^{\mathrm{T}}|^2=|E_p^{\mathrm{T}}|^2+|E_s^{\mathrm{T}}|^2$$

and

$$S_3^{+}\equiv|\hat{\epsilon}_{+}^{*}\cdot\mathbf{E}_{s,p}^{\mathrm{T}}|^2-|\hat{\epsilon}_{-}^{*}\cdot\mathbf{E}_{s,p}^{\mathrm{T}}|^2=-2\ \mathrm{Im}\,[E_s^{\mathrm{T}}E_p^{*\mathrm{T}}].$$

As a result,

$$\rho^{+}=-2\ \mathrm{Im}\left[\frac{E_s^{\mathrm{T}}E_p^{*\mathrm{T}}}{|E_p^{\mathrm{T}}|^2+|E_s^{\mathrm{T}}|^2}\right]\approx-2\ \mathrm{Im}\left[\frac{E_s^{\mathrm{T}}}{E_p^{\mathrm{T}}}\right], \tag{2}$$

where the last approximation follows because $|E_s^{\mathrm{T}}|$ is normally much smaller than $|E_p^{\mathrm{T}}|$ for the particular setup we are considering. Hence, the experimentally measured quantity is

$$\rho^{+}-\rho^{-}\approx 2\ \mathrm{Im}\left[-\frac{E_s^{\mathrm{T}}(\mathrm{detector})}{E_p^{\mathrm{T}}(\mathrm{detector})}\right]-(\mathbf{M}\rightarrow-\mathbf{M}). \tag{3}$$

The basic physics behind these equations is that tunneling electrons undergoing inelastic events via spontaneous emission produce a radiating field in the vicinity of the tip. This leads primarily to emission of *p*-polarized light, but when reflected in the surface of the magnetic sample it also gives rise to a small field component in a direction parallel to the surface due to the Kerr effect. We have thus expressed the measured MCD in terms of the field amplitudes at the detector. To facilitate the ensuing calculations, we will next relate these tip-induced fields in the detector region to complementary fields generated by sources at the detector.

B. Reciprocity theorem

In this subsection we use the reciprocity theorem to reformulate Eq. (3). The electrons tunneling inelastically between tip and sample can emit photons and are a source of electromagnetic radiation. This radiation couples to tip and sample and is finally detected far from the tip. We have previously found[12] that it is convenient to use the reciprocity theorem of classical electrodynamics[13] in such a situation because it allows the radiated field to be approximately determined by a nonretarded calculation if the wavelength of the emitted light is large compared to the relevant tip extension. This theorem essentially states that the result of a measurement is unchanged if the source and field points are interchanged. Here, the reciprocity theorem can be written as

$$\sum_j \int dV E_j^T(\mathbf{x})\ \ J_j^D(\mathbf{x}) = \sum_j \int dV E_j^D(\mathbf{x}) J_j^T(\mathbf{x}), \quad (4)$$

where j denotes the components x, y, and z. The current $\mathbf{J}^{T(D)}$ at the tip (detector) is the source for the electromagnetic field $\mathbf{E}^{T(D)}$.

Equation (4) is valid for media with time-reversal symmetry. However, a magnetic material does not fulfill this condition and one has to use a modified reciprocity theorem[13] whereby Eq. (4) can still be used provided the true medium is replaced by its complementary medium (one with reversed magnetic field). If the dielectric tensor of the real medium is ϵ_{ij}, then the complementary medium has a dielectric tensor ϵ_{ij}^c which is the transpose of ϵ_{ij}; $\epsilon_{ij}^c = \epsilon_{ji}$. The dielectric matrix has the form

$$\epsilon_{ij} = \begin{pmatrix} \epsilon_S(\omega) & \epsilon_1 \cos\phi & -\epsilon_1 \sin\gamma \sin\phi \\ -\epsilon_1 \cos\phi & \epsilon_S(\omega) & \epsilon_1 \cos\gamma \sin\phi \\ \epsilon_1 \sin\gamma \sin\phi & -\epsilon_1 \cos\gamma \sin\phi & \epsilon_S(\omega) \end{pmatrix}, \quad (5)$$

where the notation $\epsilon_1(\omega) \equiv iQ\epsilon_S(\omega)$ is sometimes used with Q being the so called magneto-optical constant and $\epsilon_S(\omega)$ is the substrate dielectric function. The angles ϕ and γ specify the direction of the applied magnetic field with respect to the surface normal and the plane of incidence. We see that the complementary medium corresponds to changing the sign of the off-diagonal components.

To a high degree of accuracy, the current between the tip and sample is spatially well-localized and perpendicular to the substrate. Thus we write

$$J_j^T(\mathbf{x}) = \hat{\mathbf{z}} J_o(\boldsymbol{\rho}, z), \quad (6)$$

where $\hat{\mathbf{z}}$ is normal to the surface, pointing inwards. The relative independence of E_z^D on position in the surface-tip region has been verified by numerical calculation[14] and is also a key feature of the models used in this paper. We can take out an average value of $\mathbf{E}^D$ in the region between tip and sample and write the right hand side of Eq. (4) as

$$E_z^D \int dV J_o(\rho, z) \equiv j_o E_z^D. \quad (7)$$

E_z^D is the perpendicular component of $\mathbf{E}^D$, with respect to the surface plane, i.e., in the z direction. The electronic current from the STM flows primarily in the normal direction with respect to the surface, thus only a perpendicular component of a ''detector-generated'' field can couple to that tunneling current.

On the left hand side of Eq. (4), we insert a current source with two components

$$\mathbf{J}^D(\mathbf{x}) = \hat{\mathbf{n}} j_n \delta(\mathbf{x} - \mathbf{x}_D), \quad (8)$$

where $\mathbf{x}_D$ is the detector position and $\hat{\mathbf{n}}$ corresponds to either the direction $\hat{\mathbf{s}}$ or $\hat{\mathbf{p}}$. Notice that these currents generate two different E_z^D, which we write as E_z^n in what follows ($n = s$ or p). Equations (4), (7), and (8) yield

$$E_n^T(\text{detector}) j_n = j_o E_z^n. \quad (9)$$

Combining Eq. (9) with Eq. (3) and also including the complementary-medium sign change we obtain

$$\rho^+ \simeq 2\ \text{Im}\left[\frac{E_z^s/j_s}{E_z^p/j_p}\right] = 2\ \text{Im}\left[\frac{E_z^s/E_s^{\text{inc}}}{E_z^p/E_p^{\text{inc}}}\right] \quad (10)$$

and ρ^- is $\rho^+(M \to -M)$. In the last line we have replaced $j_{s,p}$ by the corresponding incoming field strengths $E_{s,p}^{\text{inc}}$ since s polarization and p polarization represent two orthogonal polarization states. Thus the reciprocity theorem makes it possible to express the tip-generated field at the detector position $[E_n^T(\text{detector})]$ as the fields in the tip region generated by incoming s- and p-polarized waves.

C. Determination of fields at STM tip

In this section we model the STM tip in such a way as to include the main physical effects and to allow the development of a formalism for determining the fields at the tip. The system of tip and sample is a difficult one to treat for several reasons. Even if the tip was perfect, in the sense of having a well-characterized geometrical shape, the resulting electromagnetic field problem has relatively low symmetry. Consequently, we model the tip as a polarizable sphere of radius R, with a scalar polarizability $\alpha_o(\omega)$, situated a distance $d = R + D$ from a surface. Then we replace the sphere with a dipole at d. In this way we include the relevant physics, such as a relatively constant field in the region between tip and sample, while making the problem tractable. Since the circular polarization is a ratio between two quantities, we hope that a simpler model can capture the main features of the emitted light. A dipole model was also used to study the polar Kerr effect by Kosobukin[15] in the context of near field optics. In Sec. III we improve upon this by using the full sphere in the calculations. We consider the nonmagnetic situation in this section and introduce the magnetic substrate in Sec. II D.

Consider a sphere centered at $\mathbf{d} = (0,0,-d)$ where $-d$ is the position of the sphere outside a metal surface whose optical reflection can be described in terms of its Fresnel reflection coefficients ρ_s and ρ_p for s-polarized and p-polarized light, respectively. The tip (sphere) above the surface is *replaced* by a *point* polarizable dipole with polarizability $\alpha_o(\omega)$. The total electromagnetic field at the dipole position $\mathbf{E}(\mathbf{d}, \omega)$ can be divided into two parts $\mathbf{E}^{\text{ext}}$ and $\mathbf{E}^t$: $\mathbf{E}^{\text{ext}}$ is the solution to Maxwell equations with an incident electromagnetic field and no tip present while $\mathbf{E}^t$ is a solution when we have no incoming electromagnetic field but the induced field at the tip plays the role of a *source* term. Assume the point dipole has an induced dipole moment $\mathbf{P} = (\mathbf{P}_\parallel, P_\perp)$. The solution to the $\mathbf{E}^t$ problem can be simplified if we decompose the induced field at the tip in Fourier components parallel to the surface ($\mathbf{k}$) and note that they play the role of incoming electromagnetic fields analogous to the situation in the $\mathbf{E}^{\text{ext}}$ problem (however, we have to sum over all possible parallel wave vector components to get the total field). The (near) field from a dipole can be Fourier decomposed according to

$$\mathbf{E}(\mathbf{x}, \omega) = \int \frac{d^2k}{(2\pi)^2} \mathbf{E}(\mathbf{k}, z, \omega) e^{i\mathbf{k}\cdot\mathbf{x}}, \quad (11)$$

where $\mathbf{E}(\mathbf{k},z,\omega)$ is the analog to an ''incoming'' electromagnetic field. In our case the lowest order magnetic component is smaller than the electric field by a factor $\omega d/c \ll 1$. The total field from the dipole and its image[16] is expressed in components parallel and perpendicular to the surface as

$$\mathbf{E}_{\parallel}^{t}(\mathbf{k},z,\omega) = ip[\mathbf{E}_{\parallel}^{o}e^{ipz} + (\rho_s \hat{\mathbf{T}}\mathbf{E}_{\parallel}^{o} - \rho_p(\mathbf{1}-\hat{\mathbf{T}})\mathbf{E}_{\parallel}^{o})e^{-ipz}] \tag{12}$$

and

$$E_{\perp}^{t}(\mathbf{k},z,\omega) = -i\mathbf{k}\cdot\mathbf{E}_{\parallel}^{o}(e^{ipz} + \rho_p e^{-ipz}), \tag{13}$$

where ρ_s and ρ_p are the reflection coefficients for *s*- and *p*-polarized light scattered from the surface. In Eqs. (12) and (13) we have introduced

$$\mathbf{E}_{\parallel}^{o} = \frac{2\pi}{p}e^{ipd}\left[-\mathbf{k}P_{\perp} + p\mathbf{P}_{\parallel} + \frac{k^2}{p}\hat{\mathbf{T}}\mathbf{P}_{\parallel}\right] \tag{14}$$

and the transverse projection operator in the surface plane is $\hat{\mathbf{T}} = \mathbf{1} - \hat{\mathbf{k}}\hat{\mathbf{k}}$, where $\hat{\mathbf{k}}$ is a unit vector along $\mathbf{k}$. Furthermore $p^2 + k^2 = q^2 = \omega^2/c^2$ for the wave vector $\mathbf{q} = (\mathbf{k},p)$ of the incoming field. In order to use the reciprocity theorem above we expose the surface and the tip to an incoming electromagnetic field $\mathbf{E}^{\mathrm{inc}}$. In the absence of the tip the total field would be $\mathbf{E}^{\mathrm{ext}} = \mathbf{E}^{\mathrm{inc}} + \mathbf{E}^{\mathrm{refl}}$, where $\mathbf{E}^{\mathrm{refl}}$ is the reflected field. Upon introducing the dipole, it will develop an induced polarization

$$\mathbf{P}(\mathbf{d}) = \alpha_o(\omega)[\mathbf{E}^{\mathrm{ext}}(\mathbf{d}) + \mathbf{E}^{t}(\mathbf{d})], \tag{15}$$

where $\mathbf{d} = (0,0,-d)$ is the position of the dipole and $\mathbf{E}^{t}(\mathbf{d})$ is the image field of the polarized tip due to the presence of $\mathbf{P}$. One can show that[16] (see also Appendix A):

$$\mathbf{E}^{t}(\mathbf{d}) = F_{\parallel}\mathbf{P}_{\parallel} + F_{\perp}P_{\perp}\hat{\mathbf{z}} \tag{16}$$

for $\mathbf{P}$ in the surface plane ($\mathbf{P}_{\parallel}$) or perpendicular to it ($P_{\perp}$). We have defined the feed-back, or image functions

$$F_{\parallel} = \frac{1}{2}\int_0^{\infty} dk k \frac{e^{2ipd}}{-ip}[q^2\rho_s(k,\omega) - p^2\rho_p(k,\omega)] \tag{17}$$

and

$$F_{\perp} = \int_0^{\infty} dk k^3 \frac{e^{2ipd}}{-ip}[\rho_p(k,\omega)] \tag{18}$$

after performing an angular integration in the surface plane. The non-retarded limit for $F_{\parallel}$ and $F_{\perp}$ is obtained by letting $c \to \infty$ with the result that p is replaced by ik.

Equation (15) is a self-consistency condition on the induced dipole moment representing the tip. Solving for $\mathbf{P}$ we obtain

$$P_i = \frac{\alpha_o(\omega)}{1 - \alpha_o(\omega)F_i}E_i^{\mathrm{ext}}(\mathbf{d}), \tag{19}$$

where $i = \parallel$ and $\perp$. The denominator in Eq. (19) can be included with the field to form an effective field acting on the unperturbed tip (dipole) or it can be included with the bare polarizability α_o to form an effective polarizability. For special frequencies, the coupled system exhibits resonances when $\mathrm{Re}(\alpha_o F_i) = 1$ and P_i can be very large. An explicit demonstration of this is found[17] for a sphere outside a surface. Combining Eqs. (15) and (16) we obtain the total field at the dipole position

$$\begin{aligned}\mathbf{E}^{tot}(\mathbf{d}) &= \mathbf{P}(\mathbf{d})/\alpha_o \\ &= \mathbf{E}^{\mathrm{ext}}(\mathbf{d}) + \mathbf{E}^{t}(\mathbf{d}) \\ &\equiv \mathbf{E}^{\mathrm{ext}}(\mathbf{d}) + G_{\parallel}\mathbf{E}_{\parallel}^{\mathrm{ext}}(\mathbf{d}) + G_{\perp}\hat{z}\mathrm{E}_{\perp}^{\mathrm{ext}}(\mathbf{d}),\end{aligned} \tag{20}$$

where $G_{\parallel,\perp}\mathbf{E}^{\mathrm{ext}}$ is the field at the tip, due to the image of the tip produced by $P_{\parallel,\perp}$. We have introduced an image factor G_i defined as

$$G_{\parallel,\perp} = \frac{\alpha_o(\omega)F_{\parallel,\perp}}{1 - \alpha_o(\omega)F_{\parallel,\perp}}. \tag{21}$$

For a substrate characterized by a frequency dependent dielectric function $\epsilon_S(\omega)$ we find in the nonretarded limit

$$F_{\perp} = 2F_{\parallel} = \frac{1}{4d^3}\frac{\epsilon_S(\omega) - 1}{\epsilon_S(\omega) + 1}. \tag{22}$$

In Eq. (21), α_o contains information about the dipole resonances and $F_{\parallel,\perp}$ contains information about the surface (sample) resonances ($\epsilon_S + 1 = 0$ corresponds to surface plasmons). From Eq. (21) we see how the tip and sample couple to yield new eigenmodes at the poles of $G_{\parallel,\perp}$, and also a possible field enhancement. In this respect our model contains all the features of more refined calculations for the STM configuration.[14] For the dipole (tip), we use the polarizability for a sphere of radius R and dielectric function $\epsilon_T(\omega)$:

$$\alpha_o(\omega) = R^3\frac{\epsilon_T(\omega) - 1}{\epsilon_T(\omega) + 2}. \tag{23}$$

In this way one can also include a more accurate dielectric response of the tip, e.g., using measured values for ϵ_T. The factor 2 in the denominator is actually $(-1 + 1/n)$ where n is the so called depolarization factor. Thus we could also mimic different tip shapes by choosing different values of n.

In the following discussion we retain Eq. (20) as a generic form for the resulting field at the tip position when an incoming field is incident on the tip and the sample. Notice also that the only boundary condition matching is done in the absence of the tip. After this the self-consistency condition for the induced dipole moment [Eq. (15)] adjusts the total field strength appropriately.

D. Local field near tip with magnetic substrate

In Sec. II B we related the fields at the detector to the fields of the inverse problem where light is scattered from the tip. In the previous section we showed how the incoming field is affected by the presence of a tip outside a nonmagnetic solid. Furthermore, we expressed the fields in terms of the total field outside the substrate in the absence of the tip: $\mathbf{E}^{\mathrm{ext}}(\mathbf{d})$ in Eq. (20). Now we will calculate $\mathbf{E}^{\mathrm{ext}}(\mathbf{d})$, and also consider the changes in the reflected dipole field, in the presence of a *magnetic* sample. We first address the field felt by a tunneling electron that undergoes an inelastic event leading to the light emission.

In the previous section we calculated the induced polarization at the tip in a self-consistent manner and obtained the field at the tip position itself. A tunneling electron will not only feel the incoming field and the reflected field of the incoming light, but the tip-induced image field as well as the direct dipole field from the tip. In the region between the actual tip and substrate these fields vary only slightly since the dipole is far away from the surface, $R \gg D$. We can write the field acting on a tunneling electron as ($i\|,\perp$):

$$E_i = F_o P_i = F_o \alpha_o (1+G_i)(1+\rho_i) E_i^{\rm inc}, \tag{24}$$

where all fields represent average values in between tip and sample. F_o is a the dipole factor which gives the field strength for a given polarizability **P**. Notice that if we have no surface present $E = F_{o,\rm direct} \alpha_o E^{\rm inc}$, where $F_{o,\rm direct}$ is the direct part of F_o. We see that $(1+G)$ plays the role of a field enhancing factor for the incoming and scattered electromagnetic fields from the surface $(1+\rho)E^{\rm inc}$. α_o is a property of the tip, G depends on both the sample and the tip, and ρ is a property of the sample.

To determine **P** we first have to calculate the reflected field from a magnetic surface and such a reflection involves the magneto-optic Kerr effect. For general angles between applied magnetic field, surface plane and plane of incidence there is an excellent treatment by Zak *et al.*[18] which is very useful when dealing with light reflection from a magnetic solid. For a general magnetic configuration the proper form of the dielectric matrix was given in Eq. (5). The off-diagonal elements of this tensor carry the information about the Kerr effect. The origin of the nondiagonal components is a coupling between the spin of the electrons in the solid and their orbital momentum due to the atomic potentials (spin-orbit coupling). The first theoretical calculations of this effect were carried out by Hulme[19] and Argyres.[20] Equation (5) assumes that the dielectric tensor is diagonal when $\epsilon_1(\omega) = 0$ (this approximation can be relaxed but it does not influence our final conclusions).

For the applied magnetic field in the surface plane we can use Eq. (5) for the general dielectric tensor with $\phi = \pi/2$ and one angle (γ) suffices to specify the direction of **M** with respect to the plane of incidence. The dielectric matrix in Eq. (5) then simplifies to

$$\epsilon_{ij} = \begin{pmatrix} \epsilon_S(\omega) & 0 & -\epsilon_1(\omega)\sin\gamma \\ 0 & \epsilon_S(\omega) & \epsilon_1(\omega)\cos\gamma \\ \epsilon_1(\omega)\sin\gamma & -\epsilon_1(\omega)\cos\gamma & \epsilon_S(\omega) \end{pmatrix}. \tag{25}$$

We use this result in the Zak matrix multiplication method, together with an expansion to first order in $\epsilon_1(\omega)$, since the off-diagonal elements are small compared to $\epsilon_S(\omega)$ $[|\epsilon_1(\omega)/\epsilon_S(\omega)| \ll 1]$. However, these matrix elements provide a coupling between *s* polarization and *p* polarization leading to a nonzero Kerr rotation. For *s*-polarized incident light (along *x* direction), $E_s^{\rm inc}$, our analysis gives the reflection coefficient for *s*-polarized light to lowest order in $\epsilon_1(\omega)$, as

$$\rho_s = \frac{p - p_S}{p + p_S} + O(\epsilon_1^2) \tag{26}$$

which is the standard Fresnel result.[11] $p = \sqrt{q^2 - k^2}$ and for $q > k, k = q \sin\theta$ with θ being the angle of incidence. For $k \gg q, p \to ik$. $p_S = \sqrt{q^2 \epsilon_S(\omega) - k^2}$, with $\epsilon_S(\omega)$ defined above. Finally $q = \omega/c$, where c is the light velocity. Apart from the direct reflection of *s*-polarized light there is a small but crucial conversion from *s*- to *p*-polarized light with a reflection coefficient

$$\rho_{ps} = \epsilon_1(\omega) \frac{kpq}{p_S(p+p_S)(\epsilon_S p + p_S)} \sin\gamma + O(\epsilon_1^2) \equiv \rho_L \sin\gamma. \tag{27}$$

It is proportional to $\epsilon_1(\omega)$ since it comes from the off-diagonal response. For large $\epsilon_S, \rho_{ps} \propto \epsilon_1/\epsilon_S^2$. With Zak's field conventions, Eq. (27) corresponds to a reflected field amplitude, $-\rho_{ps} E_s^{\rm inc} \sin\theta$, in the *z* direction. It is clear from Eq. (27) that a general direction of the applied magnetic field in the surface plane corresponds to replacing $\epsilon_1(\omega)$ in the strictly longitudinal configuration ($\gamma = \pi/2$) by $\epsilon_1(\omega)\sin\gamma$ for the *s*-polarized case. Changing the direction of **M** ($\gamma \to \gamma + \pi$) changes the sign of ρ_{ps} as it should.

Repeating the same analysis as above for *p*-polarized incoming light we find, to lowest order in the off-diagonal elements:

$$\rho_p = \frac{\epsilon_S p - p_S}{\epsilon_S p + p_S} + \rho_T \cos\gamma + O(\epsilon_1^2) \tag{28}$$

with

$$\rho_T \equiv \frac{-2\epsilon_1(\omega) pk}{[\epsilon_S(\omega) p + p_S]^2}. \tag{29}$$

The corresponding reflection coefficient for *p*- to *s*-polarized conversion is $\rho_{sp} = -\rho_{ps}$. The first term in Eq. (28) is the standard Fresnel reflection coefficient for a nonmagnetic solid.[11] For later use we need the nonretarded limit of Eqs. (28) and (29), viz.:

$$\rho_p^o = \frac{\epsilon_S(\omega) - 1}{\epsilon_S(\omega) + 1} + \rho_T^o \cos\gamma + O(\epsilon_1^2), \tag{30}$$

where

$$\rho_T^o = \frac{2i\epsilon_1(\omega)}{[\epsilon_S(\omega) + 1]^2}. \tag{31}$$

The first term in Eq. (30) is the classical image factor for a solid with dielectric function $\epsilon_S(\omega)$.

Making use of the formalism of Zak *et al.*,[18] we find that for an irradiated magnetic surface we can make the following replacements with respect to the nonmagnetic situation:

$$\rho_s \to \rho_s + \rho_{sp} \equiv \rho_s - \rho_L \sin\gamma \tag{32}$$

and

$$\rho_p \to \rho_p + \rho_{ps} \equiv \rho_p + \rho_L \sin\gamma + \rho_T \cos\gamma. \tag{33}$$

ρ_L is defined in Eq. (27) and ρ_T is defined in Eq. (29).

The change in reflection factors for a magnetic surface compared to the nonmagnetic situation will also affect the

reflected field from the tip. We are interested in the near field and therefore take the nonretarded limit of ρ_L; ρ_L^o:

$$\rho_L^o = \frac{q\epsilon_1(\omega)}{2k[\epsilon_S(\omega)+1]} \tag{34}$$

to lowest order. Notice that ρ_p has a finite value $[\rho_p^o + \rho_T^o \cos\gamma$, cf. Eq. (30)] in this limit and that ρ_s vanishes as $O[(q/k)^2]$. In what follows, we neglect $\rho_L^o \propto q/k$ compared to ρ_T^o since $k \gg \omega/c$ in the nonretarded limit. Repeating the previous treatment for a magnetic material one finds [by letting ρ_s and ρ_p be transformed according to Eqs. (32) and (33)] that Eq. (16) is replaced by (see Appendix A)

$$\mathbf{E}_\parallel^{\mathrm{loc}}(\mathbf{d}) = F_\parallel \mathbf{P}_\parallel - F_T P_\perp (\hat{\mathbf{z}} \times \hat{\mathbf{M}}) \tag{35}$$

and

$$E_\perp^{\mathrm{loc}}(\mathbf{d}) = F_\perp P_\perp + F_T \mathbf{P}_\parallel \cdot (\hat{\mathbf{z}} \times \hat{\mathbf{M}}), \tag{36}$$

where $\hat{\mathbf{M}}$ is a unit vector in the surface plane in the direction of $\mathbf{M}$ and $\hat{\mathbf{z}}$ is normal to the metal and directed towards it. The coupling factor due to the off-diagonal response of the medium F_T is given by (nonretarded limit)

$$F_T \equiv \frac{1}{2i}\int dk k^2 \rho_T^o(k,\omega) e^{-2kd} = \frac{1}{4d^3}\frac{\epsilon_1(\omega)}{[\epsilon_S(\omega)+1]^2} \tag{37}$$

using ρ_T^o from Eq. (31) in the last line. The physics behind the structure of the above equations is the following. A perpendicular dipole [Eq. (35)] provides an electromagnetic field which is reflected in the surface and gives an induced electric field and dipole component parallel to the surface (due to Kerr response, through F_T) and perpendicular to the magnetization $\mathbf{M}$. A parallel dipole likewise is reflected and provides an induced perpendicular field and dipole, due to F_T. If both $\mathbf{M}$ and $\mathbf{P}_\parallel$ are parallel there is however no such contribution.

E. Theoretical results

We have now developed all the necessary ingredients for calculating the circular polarization from Eq. (10). First consider the case of incident *s*-polarized light at an angle θ. A field $E_s^{\mathrm{inc}}\hat{\mathbf{s}}$ (along the *x* direction, $\hat{\mathbf{s}} = \hat{\mathbf{x}}$) sets up a parallel polarization of the tip

$$\mathbf{P}_\parallel = \alpha_o[(1+\rho_s)E_s^{\mathrm{inc}}\hat{\mathbf{x}} + F_\parallel \mathbf{P}_\parallel - F_T P_\perp (\hat{\mathbf{z}} \times \hat{\mathbf{M}})]. \tag{38}$$

Equations (15) and (35) have been used to derive Eq. (38). There is also a perpendicular polarization

$$P_\perp = \alpha_o[-\sin\theta \rho_{ps}^{(-M)} E_s^{\mathrm{inc}} + F_\perp P_\perp + F_T \mathbf{P}_\parallel \cdot (\hat{\mathbf{z}} \times \hat{\mathbf{M}})]. \tag{39}$$

In the first term we have indicated that the conversion coefficient ρ_{ps} is now, due to the exact form of the reciprocity theorem, to be evaluated in a situation which is the same as the one considered above if we change the sign of *M*. The Kerr coupling between the induced dipole moments of the tip is included through the coupling function F_T. In Eq. (39) the first term is the *z*-component Kerr field set up by the incoming *s*-polarized light. The second term is the image from the tip-induced polarization perpendicular to the surface. Finally the third term is the image from the parallel induced dipole set up by the incoming s-polarized wave [Eq. (38)] which is converted to a perpendicular component by the nondiagonal response of the substrate. The latter is described through F_T which is given above. Neglecting F_T in Eq. (38), substituting the resulting expression in Eq. (38) for $\mathbf{P}_\parallel$ into Eq. (39) and using Eqs. (15), (20), and (21) gives the field experienced by an electron between tip and sample to lowest order in F_T [cf., Eq. (24)]:

$$E_z^s = (1+G_\perp)(\alpha_o F_o)[\rho_L \sin\theta - (1+\rho_s)G_\parallel K(\omega)]E_s^{\mathrm{inc}} \sin\gamma \tag{40}$$

due to the incoming field E_s^{inc}. We have used $\hat{\mathbf{x}} \cdot (\hat{\mathbf{z}} \times \hat{\mathbf{M}}) = -\sin\gamma$ and defined

$$K(\omega) \equiv F_T/F_\parallel = \frac{2\epsilon_1(\omega)}{[\epsilon_S^2(\omega)-1]}. \tag{41}$$

Note that the right hand side of Eq. (40) is proportional to $\sin\gamma$, the orientation of the magnetization in the surface plane; longitudinal polarization providing for the maximum field strength.

E_z^s in Eq. (40) is the major part of the average field in the *z* direction in the narrow region between tip and sample, created by the incoming *s*-polarized field of magnitude E_s^{inc}. The first factor in Eq. (40) is understood as follows; an incoming *s*-polarized field of magnitude E_s^{inc} undergoes a Kerr rotation and a field proportional to ρ_L is created in the *z* direction. The tip acquires a *z* component of polarization and radiates. This radiation is also reflected back to the tip by the surface, thus the tip sees its own image giving a contribution $G_\perp \rho_L$. The total field at the tip is the original field plus the image field. Thus, $G_\perp$ is an image (enhancement) factor due to the polarization of the tip in the $\hat{\mathbf{z}}$ direction. The quantity $G_\perp$ depends on the dielectric properties of the tip, the metal, the distance between them, and on the geometry of the tip.

The second term in Eq. (40) is explained as follows. $(1+\rho_s)E_s^{\mathrm{inc}}$ is the field at the tip due to light that falls directly on the tip plus light that is reflected from the metal surface. The tip is then polarized in a direction parallel to the surface and it radiates. This *s*-polarized radiation is reflected in the surface and undergoes a Kerr rotation so that it develops a *z*-component. The term $G_\parallel K$ is the analogue of ρ_L in the first term. Once a field is created in the *z* direction it is enhanced by the factor $(1+G_\perp)$ in front.

Performing the above calculation for an incoming *p*-polarized wave with amplitude E_p^{inc} and working only to zeroth order in the off-diagonal dielectric matrix [since both terms in Eq. (40) above for *s*-polarized light are already of first order in $\epsilon_1(\omega)$] we find

$$E_z^p = -(1+G_\perp)(\alpha_o F_o)(1+\rho_p)\sin\theta E_p^{\mathrm{inc}}, \tag{42}$$

where $\sin\theta E_p^{\mathrm{inc}}$ is the field that falls directly on the tip and $\rho_p \sin\theta E_p^{\mathrm{inc}}$ is the field at the tip that is reflected from the surface. The total field is enhanced by the same factor $(1+G_\perp)$ as discussed above.

With the use of Eqs. (3), (10), (40), (41), and (42) this leads to the following expression for the magnetic circular dichroism, to lowest order in $\epsilon_1(\omega)$:

$$\rho^+ - \rho^- = 4 \sin\gamma \, \mathrm{Im}\left[-\frac{\rho_L}{1+\rho_p} + G_\parallel \left(\frac{1+\rho_s}{1+\rho_p}\right) \frac{K(\omega)}{\sin\theta}\right], \tag{43}$$

Note that the light enhancement factor $G_\perp$ from the perpendicular field component drops completely out of the problem as does the dipolar factor F_o so the ratio does not depend on where in the junction the light emission takes place. In Sec. III we will make a more realistic estimate of Eq. (43) for the magnitude of the magnetic circular dichroism. However, let us already here say that the fact that $G_\perp$ drops out of the dipole-model calculation gives one hint to why this model, as we will see, yields results for the magnetic circular dichroism that are of the right order of magnitude although the field enhancement (described by $G_\perp$) in the dipolar model may be very different from that calculated in the improved model.

III. IMPROVED THEORETICAL MODEL

Here we outline a calculation of the tip-induced MCD signal within a model geometry where the STM tip is represented by a sphere characterized by a bulk dielectric function $\epsilon_T(\omega)$. This allows for a much better description of the tip polarization. Most of the calculational details are deferred to Appendix B.

We set out to determine E_z^s in Eq. (10), and this is achieved via the following four steps. (i) The incoming *s*-polarized wave is reflected by the sample surface. This yields a total field E^{ext} parallel to the surface. (ii) That field in turn drives the model tip so that it sends out a field that is reflected back and forth between the tip and sample. In this step, we need to extract the part of the field that the tip sends onto the sample. (iii) Next, due to the off-diagonal elements of the sample dielectric tensor, part of the electric field parallel to, and incident on the sample is converted to a field perpendicular to the surface as follows from Eq. (30). It is only at this stage that the magnetic properties of the sample enters the calculation. (iv) In the last step, we calculate the degree to which the converted electric field is enhanced inside the tip-sample cavity.

Step (i). With an *s*-polarized wave incident from the right (positive y) with electric field E_s^{inc}, the Fresnel formulas yields a total field just outside the sample surface given by

$$\mathbf{E}^{\mathrm{ext}} = \mathbf{E}_s^{\mathrm{inc}}(1+\rho_s) = \hat{x} E_s^{\mathrm{inc}} \frac{2p}{p+p_S}. \tag{44}$$

Thus before introducing the model tip into the problem, we have an electric field outside the sample that can be described (in the nonretarded limit) by the scalar potential

$$\phi^{\mathrm{ext}} = -xE^{\mathrm{ext}}, \tag{45}$$

where $E^{\mathrm{ext}} = E_s^{\mathrm{inc}}[2p/(p+p_S)]$.

Step (ii). Once the model tip is introduced into the problem ϕ^{ext} alone is no longer a solution of Laplace's equation in the region above the sample, instead another contribution ϕ_{ind} has to be added. Using the appropriate boundary conditions for the **E** and **D** fields at the sample and tip surfaces ϕ_{ind} can be determined. In the following, we only want to keep the part of ϕ_{ind} that the tip sends onto the sample. As we will see in Appendix B, this separation can be done by a simple inspection of the solution.

Step (iii). We proceed to find the field that is reflected from the sample surface due to the second term in Eq. (30); this is the converted field $\mathbf{E}^{\mathrm{conv}}$. Equation (30) defines a surface response function $\chi(\mathbf{k},\omega) = \rho_p^0$, which in terms of incident and reflected electrostatic potentials is defined as the ratio $[-\phi^{\mathrm{refl}}(\mathbf{k},\omega)/\phi^{\mathrm{inc}}(\mathbf{k},\omega)]$. A further analysis shows that within a nonretarded treatment there is a local relation between $\hat{x}\cdot\mathbf{E}_{\mathrm{ind}}^{\mathrm{inc}}$ and $\hat{z}\cdot\mathbf{E}^{\mathrm{conv}}$,

$$E_z^{\mathrm{conv}}(\boldsymbol{\rho}) = \frac{2\epsilon_1(\omega)}{[\epsilon_S(\omega)+1]^2}[\hat{x}\cdot\mathbf{E}_{\mathrm{ind}}^{\mathrm{inc}}(\boldsymbol{\rho})]. \tag{46}$$

Step (iv). In this final step, we calculate the enhancement of the converted field due to the presence of the model tip. The converted field discussed above can be represented in terms of a scalar potential ϕ^c. Again, with the tip present, ϕ^c alone does not solve Laplace's equation; it must be supplanted by another contribution ϕ_{ind}^c. The calculation determining ϕ_{ind}^c is completely analogous to the one carried out in Ref. 12, the only difference being that ϕ^c is the driving ''force'' in the present case. Having found ϕ^c and ϕ_{ind}^c, we evaluate the corresponding electric field on the symmetry axis. This is the tip-induced contribution to E_z^s appearing in Eq. (10).

IV. NUMERICAL RESULTS AND DISCUSSION

We now present numerical results for the dipole model of the tip based on the expression in Eq. (43), and for the sphere model of the tip discussed in Sec. III. We use experimental optical data for the dielectric functions of the tip and the sample. The off diagonal matrix elements of the sample dielectric function $\epsilon_1(\omega)$ are obtained from magneto-optic Kerr effect measurements. The literature contains many detailed calculations and measurements of the Kerr effect (no tip present). The Kerr effect is an optics effect caused by the spin-orbit interaction that was discovered in the last century. The spin-orbit interaction is small in Fe and Co because the orbital momentum in $3d$ metals is small. It is only in this century that a microscopic theory has emerged.[19–22] The Kerr effect has recently been calculated by a number of groups for a variety of elements and compounds (see, e.g., Gasche *et al.* and Delin *et al.*[23,24]). Similarly, on the experimental side there have been a number of measurements from those of Krinchik and Artem'ev,[25] whose results we use to obtain $\epsilon_1(\omega)$, to the recent results of Weller *et al.*[26] (see also Ref. 27).

Equation (43), derived for the dipole model, consists of two terms; the first corresponds to the direct Kerr rotation by the sample and the second to the Kerr rotation of the light produced by the radiating polarization of the STM tip as previously discussed. We will refer to the two effects as the substrate Kerr effect and the tip Kerr effect.

In order to use the dipole model to make an estimate of the tip-induced Kerr effect we calculate $G_\parallel$ from Eqs. (21), (22), and (23). The distance between the surface and the tip (i.e., from the surface to the sphere) is very small compared to the tip radius so that $d \sim R$ in Eqs. (22) and (23) and $G_\parallel$ is

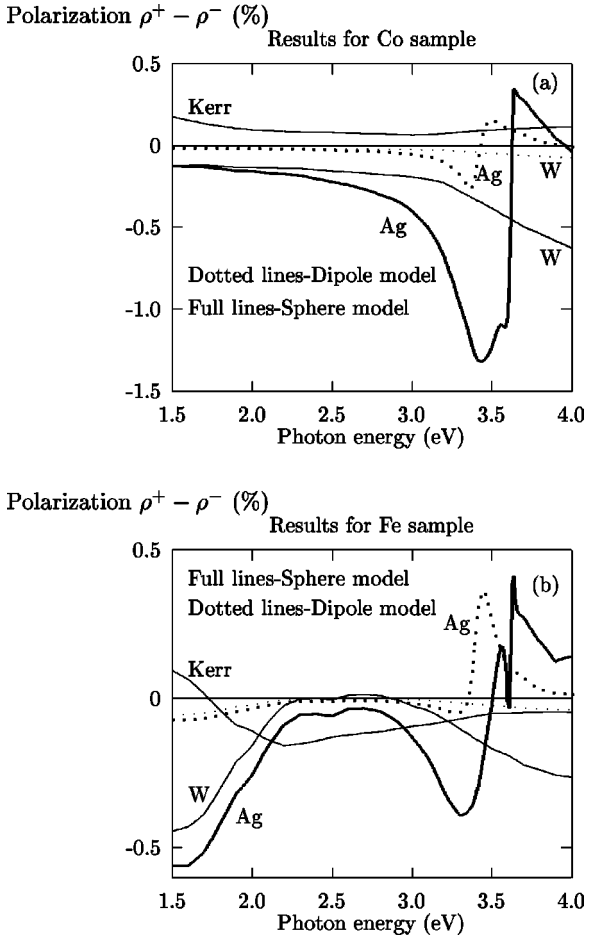

FIG. 2. Calculated results for the circular polarization for (a) a Co sample, and (b) a Fe sample. Each of the figures present results obtained from both the dipole model (dotted curves) and the improved (sphere) model (full curves), moreover, results corresponding to Ag and W tips (as indicated next to the curves) as well as the substrate Kerr contribution are displayed in both panels. In the sphere-model calculation we used $R=300$ Å for the tip radius and $D=5$ Å for the tip-sample separation. The sphere model in general gives a larger tip-induced contribution to the degree of polarization, nevertheless the results obtained with the two different methods have many qualitative features in common.

determined by using experimental values for the dielectric functions of the tip and sample. When comparing our results in Eq. (43) with the experiments of Vázques de Parga and Alvarado[4] and Pierce *et al.*,[7] we immediately recognize that in the longitudinal configuration that they use, $\hat{\mathbf{s}}$ and $\hat{\mathbf{M}}$ are perpendicular to each other so that $\sin\gamma=1$.

Considering the improved (sphere) model, the quantities entering Eq. (10) were calculated as outlined in Sec. III and Appendix B. As for the model geometry we here used a tip-sample distance $D=5$ Å, and the tip radius R was set to 300 Å.

The results of the calculations for the degree of circular polarization, $\rho^+-\rho^-$, are presented in Fig. 2. Figure 2(a) displays the results obtained with a Co sample, while Fig. 2(b) shows the results relevant for a Fe sample. In each panel, the results for the substrate Kerr contribution (one single curve) and the tip-induced contribution (four curves) to the degree of polarization are presented separately. The tip-induced degree of polarization has been calculated for Ag and W tips, respectively, using either the dipole model or the sphere model. The sphere model gives a larger degree of circular polarization than the dipole model, because it is a better description of the local electromagnetic interaction between the tip and the sample. In our calculational schemes, the tip-induced contribution ultimately results from a Kerr rotation of the electromagnetic fields incident from the tip onto the sample. The strength of the incident field is determined by how strongly the tip is excited by the incoming *s* wave as well as by waves reflected back and forth between the tip and sample. The sphere model allows for a more complete treatment of the repeated reflections than the dipole model, and therefore gives larger values for $\rho^+-\rho^-$. The dipole approximation works fairly well because the circular polarization is given by the ratio of *p* and *s* electric fields.

The effects of the tip-sample interaction is particularly pronounced for a silver tip. An isolated sphere has a dipole-plasmon resonance when the dielectric function $\epsilon_T(\omega)=-2$. For silver, the dielectric function approaches this value near 3.5 eV. Then the model tip becomes highly polarizable and the feedback mechanism, the waves reflected between the tip and the sample, described above becomes even more effective. In connection with this the electromagnetic response functions that enter our calculations undergo large phase shifts so that $\rho^+-\rho^-$ changes sign one or several times.[28] The relatively small magnitude of the results for the MCD is due to the factor $(\epsilon_S+1)^2$ in the denominator in Eqs. (31) and (46). Since ϵ_S for both Co and Fe is rather large this suppresses the MCD signal. From bulk arguments one could have assumed that the circular dichroism should be proportional to ϵ_1/ϵ_S. However, the presence of the surface changes the magnitude of both the field going into the solid to be Kerr rotated and the resulting field going out again; in both cases with a factor $1/(\epsilon_S+1)$.

It is immediately clear that within the model we have considered, there is no explanation for the large values for the degree of light polarization found by Vázques de Parga and Alvarado.[4] The calculated results are an order of magnitude or more smaller than the experimental results found in Ref. 4. Even though we use a rather simple model for the geometry as compared with the complicated, and to a certain degree unknown geometry of a real STM tip, we cannot see how this could make up for the very large difference between experimental and theoretical results. Varying the geometry parameters within reasonable limits (within a nonretarded formulation the results depend only on R/D) can change the calculated degree of polarization by a factor of 2 at most. This is also the case when using different sets of optical data for the dielectric functions entering. On the other hand, our calculated results are consistent with the experimental results found by Pierce *et al.*[7] on Fe samples. Our results are also small compared to those obtained in the calculations of Majlis *et al.*,[5] some of the reasons for this are given in a footnote.[29]

Our results are not affected by the assumption of a bulk sample compared to the very thin Co (100Å) film on Au[4], provided it can still be described with bulk dielectric data. Calculations by Moog *et al.*[30] indicate that there are no fundamental changes in actual numbers for films ranging in thickness between 100 and 400 Å, except a slight enhance-

ment of the Kerr parameters. Stray fields from domains are not strong enough to affect the circular polarization.

ACKNOWLEDGMENTS

The research of two of us (S.P.A. and P.J.) is supported by grants from the Swedish Natural Science Research Council (NFR). We appreciate comments from and discussions with Dan Pierce, Angela Davies, Mark Stiles, Robert Celotta, G. Mukhopadhyay, Anna Delin, Egidijus Anisimovas, and J. Zak.

APPENDIX A

In this appendix we show how to evaluate the different angular integrations required in averaging the local dipole field over a magnetic surface. We first have a look at the integrations for the nonmagnetic case. In this instance we have three types of integrals appearing $\int d^2k(\hat{\mathbf{T}}\cdot\mathbf{E}_\parallel^o)$, $\int d^2k(\mathbf{k}\cdot\mathbf{E}_\parallel^o)$, and $\int d^2k\mathbf{E}_\parallel^o$. They can be expressed in terms of the three integrals $\int d^2k\hat{\mathbf{k}}$, $\int d^2k(\hat{\mathbf{k}}\cdot\mathbf{P}_\parallel)$ and $\int d^2k[\hat{\mathbf{k}}(\hat{\mathbf{k}}\cdot\mathbf{P}_\parallel)]$. Performing the angular integration we find that the first integral is identically zero. Since the second integral is $\mathbf{P}_\parallel$ dotted with the first integral it also vanishes. This leaves the third integral (where φ is the angular variable):

$$\int \frac{d\varphi}{2\pi}\hat{\mathbf{k}}(\hat{\mathbf{k}}\cdot\mathbf{P}_\parallel)=\frac{1}{2}\mathbf{P}_\parallel. \tag{A1}$$

This result is obtained by expressing $\hat{\mathbf{k}}$ as $\hat{\mathbf{x}}\cos\varphi+\hat{\mathbf{y}}\sin\varphi$ and $\hat{\mathbf{k}}\cdot\mathbf{P}_\parallel=P_x\cos\varphi+P_y\sin\varphi$.

In the magnetic case we have two extra angular factors in the integrand compared to the nonmagnetic case; $\sin\gamma$ and $\cos\gamma$. Expressed in terms of $\hat{\mathbf{k}}$ they are $\hat{\mathbf{k}}\cdot\hat{\mathbf{M}}$ and $\hat{\mathbf{z}}\cdot(\hat{\mathbf{M}}\times\hat{\mathbf{k}})$, where $\hat{\mathbf{M}}$ is a unit vector in the direction of the applied magnetic field. Repeating the same steps as above we find that all integrals can be expressed in terms of the following four integrals: $\int d^2k[\hat{\mathbf{z}}\cdot(\hat{\mathbf{M}}\times\hat{\mathbf{k}})]$, $\int d^2k\hat{\mathbf{k}}[\hat{\mathbf{z}}\cdot(\hat{\mathbf{M}}\times\hat{\mathbf{k}})]$, $\int d^2k\{(\hat{\mathbf{k}}\cdot\mathbf{P}_\parallel)[\hat{\mathbf{z}}\cdot(\hat{\mathbf{M}}\times\hat{\mathbf{k}})]\}$, and $\int d^2k\{\hat{\mathbf{k}}(\hat{\mathbf{k}}\cdot\mathbf{P}_\parallel)[\hat{\mathbf{z}}\cdot(\hat{\mathbf{M}}\times\hat{\mathbf{k}})]\}$. The first and last integrals vanishes since they are odd in $\hat{\mathbf{k}}$. The second integral becomes $\frac{1}{2}(\hat{\mathbf{z}}\times\hat{\mathbf{M}})$ using Eq. (A1). For the third integral we obtain

$$\int \frac{d\varphi}{2\pi}(\hat{\mathbf{k}}\cdot\mathbf{P}_\parallel)[\hat{\mathbf{z}}\cdot(\hat{\mathbf{M}}\times\hat{\mathbf{k}})]=\frac{1}{2}\mathbf{P}_\parallel\cdot(\hat{\mathbf{z}}\times\hat{\mathbf{M}}) \tag{A2}$$

again expressing the different vectors in $\hat{\mathbf{x}}$ and $\hat{\mathbf{y}}$ components and using Eq. (A1). With the use of these results it is a straightforward manipulation to arrive at Eqs. (35) and (36).

APPENDIX B

This appendix explains the calculations outlined in Sec. III in more detail. To carry them out we use bispherical coordinates,[31] furthermore, to facilitate the connection with similar, earlier calculations by us[12] and others,[32,33] we also introduce another Cartesian coordinate system (x',y',z') in which x' and z' are reversed compared with x and z, see Fig. 3. The bispherical coordinates (β,α,φ') are defined by

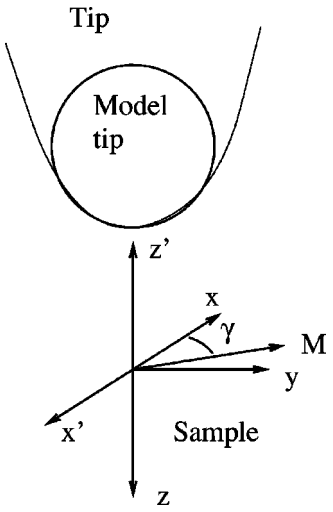

FIG. 3. Schematic illustration of the coordinate system used in the improved model calculation.

$$z'=\frac{a\sinh\beta}{\cosh\beta-\cos\alpha},\quad x'+iy'=\frac{a\sin\alpha\, e^{i\varphi'}}{\cosh\beta-\cos\alpha}. \tag{B1}$$

Both the sample surface $(z'=0,\beta=0)$ and the sphere

$$\beta=\beta_0=\ln[1+(D+a)/R]$$

are constant β surfaces. The length scale is set by the parameter

$$a=\sqrt{D^2+2RD}.$$

Let us embark on the calculations described in Sec. III. Step (i) is a straightforward application of the Fresnel formulas that yields an external potential $\phi^{\text{ext}}=-xE^{\text{ext}}=x'E^{\text{ext}}$ [see Eq. (45)] describing the electric field of an *s* polarized wave reflected off the sample surface. In the bispherical coordinates this potential can be written

$$\phi^{\text{ext}}=-E^{\text{ext}}\sqrt{8}a\sqrt{\cosh\beta-\cos\alpha}\times\sum_1^\infty e^{-(n+1/2)|\beta|}P_n^1(\cos\alpha)\cos\varphi'. \tag{B2}$$

Proceeding to step (ii), we introduce the induced potential ϕ_{ind}, and make the ansatz

$$\phi_{\text{ind}}=-\sqrt{8}aE^{\text{ext}}\sqrt{\cosh\beta-\cos\alpha}\times\sum_1^\infty F_n(\beta)P_n^1(\cos\alpha)\cos\varphi'. \tag{B3}$$

In the sample $(\beta\leqslant 0)$, the function $F_n(\beta)$ is given by

$$F_n(\beta)=(A_n+B_n)e^{(n+1/2)\beta}, \tag{B4a}$$

in the tip $(\beta\geqslant\beta_0)$

$$F_n(\beta)=(A_ne^{(2n+1)\beta_0}+B_n)e^{-(n+1/2)\beta}, \tag{B4b}$$

and finally, *between* the sample and tip $(0\leqslant\beta\leqslant\beta_0)$

$$F_n(\beta)=A_ne^{(n+1/2)\beta}+B_ne^{-(n+1/2)\beta}. \tag{B4c}$$

Thus, $F_n, \phi_{\rm ind}$, and therefore the tangential **E** field is continuous across the tip and sample interfaces. From the form of Eq. (B4c) it is clear that the field that the tip sends onto the sample is contained in the A_n terms; these fields decay exponentially as one goes away from the tip.

To determine the coefficients, A_n and B_n we must also demand that the displacement field perpendicular to the sample and tip surfaces is continuous across these interfaces. At the sample this means that

$$\epsilon_S \frac{\partial \phi_{\rm ind}}{\partial \beta}\bigg|_{\beta=0-} = \frac{\partial \phi_{\rm ind}}{\partial \beta}\bigg|_{\beta=0+} \tag{B5}$$

(here ϵ_S is the sample dielectric function), which yields

$$B_n = -\chi_S A_n, \tag{B6}$$

where the sample surface response function

$$\chi_S = \frac{\epsilon_S - 1}{\epsilon_S + 1}. \tag{B7}$$

Note that the contribution to $D_\perp$ coming from $\phi^{\rm ext}$ is already continuous since the external potential results from using the Fresnel formulas. At the tip-vacuum interface ($\beta=\beta_0$), both $\phi_{\rm ind}$ and $\phi^{\rm ext}$ must be considered in the boundary condition for $D_\perp$. This yields an equation system involving the coefficients A_n

$$U_n^s A_n + V_n^s A_{n-1} + W_n^s A_{n+1} = S_n, \tag{B8}$$

where

$$U_n^s = -(2n+1)\cosh\beta_0 \,(e^{(n+1/2)\beta_0} - \chi_S \chi_T e^{-(n+1/2)\beta_0}) + \sinh\beta_0 \,\chi_T (e^{(n+1/2)\beta_0} - \chi_S e^{-(n+1/2)\beta_0}), \tag{B9a}$$

$$V_n^s = (n-1)(e^{(n-1/2)\beta_0} - \chi_S \chi_T e^{-(n-1/2)\beta_0}), \tag{B9b}$$

$$W_n^s = (n+2)(e^{(n+3/2)\beta_0} - \chi_S \chi_T e^{-(n+3/2)\beta_0}), \tag{B9c}$$

and

$$S_n = -\chi_T \{e^{-(n+1/2)\beta_0}[\sinh\beta_0 - (2n+1)\cosh\beta_0] + (n-1)e^{-(n-1/2)\beta_0} + (n+2)e^{-(n+3/2)\beta_0}\}. \tag{B9d}$$

One arrives at these equations through a procedure that is completely analogous to the one used in earlier calculations.[12,32] Solving Eq. (B8) for the A_n coefficients, we can determine the tip-induced potential *incident* on the sample,

$$\phi_{\rm ind}^{\rm inc} = -\sqrt{8}\, a E^{\rm ext} \sqrt{\cosh\beta - \cos\alpha} \times \sum_1^\infty A_n e^{(n+1/2)\beta} P_n^1(\cos\alpha)\cos\varphi'. \tag{B10}$$

Next, we have to consider the electric field conversion at the sample surface due to the off-diagonal components of the dielectric tensor in Eq. (25). In the primed coordinate system, it takes the form

$$\epsilon'_{ij} = \begin{pmatrix} \epsilon_S(\omega) & 0 & -\epsilon_1(\omega)\sin\gamma \\ 0 & \epsilon_S(\omega) & -\epsilon_1(\omega)\cos\gamma \\ \epsilon_1(\omega)\sin\gamma & \epsilon_1(\omega)\cos\gamma & \epsilon_S(\omega) \end{pmatrix}. \tag{B11}$$

Let us use this to calculate the modified sample surface response function. If a potential

$$\phi^{\rm inc} = e^{i\mathbf{k}\cdot\boldsymbol{\rho}} e^{kz'} e^{-i\omega t} \tag{B12}$$

acts on the sample, its response yields another contribution to the potential above the surface

$$\phi^{\rm refl} = -\chi_S(\mathbf{k},\omega) e^{i\mathbf{k}\cdot\boldsymbol{\rho}} e^{-kz'} e^{-i\omega t}, \tag{B13}$$

where $\chi_S(\mathbf{k},\omega)$ is the surface response function. Combining these two contributions to the potential with a solution to Laplace's equation inside the sample

$$\phi^{\rm tr} = T(\mathbf{k},\omega) e^{i\mathbf{k}\cdot\boldsymbol{\rho}} e^{kz'} e^{-i\omega t}, \tag{B14}$$

and applying the usual boundary conditions, we obtain using Eq. (B11) that

$$\chi_S(\omega) = \frac{\epsilon_S - 1}{\epsilon_S + 1} + \frac{2i\epsilon_1 \sin(\gamma + \varphi'_k)}{(\epsilon_S+1)^2}, \tag{B15}$$

where φ'_k is the angle between $\mathbf{k}$ and $\hat{x}'$.

The second term in Eq. (B15) is our main concern; it governs the electric field conversion at the surface of the magnetic sample. In view of Eq. (B15) we write the potential corresponding to the converted field as

$$\phi^{\rm conv}(\mathbf{k}) = -\frac{2i\epsilon_1(\omega)}{(\epsilon_S+1)^2} \sin(\gamma + \varphi'_k)\, \phi_{\rm ind}^{\rm inc}(\mathbf{k}). \tag{B16}$$

Since we do not know the Fourier transform $\phi_{\rm ind}^{\rm inc}(\mathbf{k})$ we cannot immediately use this relation. However, specializing to the longitudinal configuration ($\gamma = \pi/2$) and using the fact that on the sample surface, $\phi_{\rm ind}^{\rm inc} = f(\rho)\cos\varphi'$ (ρ is the distance to the symmetry axis), one can show that with $\mathbf{M} = M\hat{y}'$ there is a local relation between $\hat{x}'\cdot\mathbf{E}_{\rm ind}^{\rm inc}$ and $\hat{z}'\cdot\mathbf{E}^{\rm conv}$,

$$E_{z'}^{\rm conv}(\boldsymbol{\rho}) = \frac{2\epsilon_1(\omega)}{(\epsilon_S+1)^2}[\hat{x}'\cdot\mathbf{E}_{\rm ind}^{\rm inc}(\boldsymbol{\rho})]. \tag{B17}$$

The calculation leading to Eq. (B17) also shows that both these fields can be written on the form $f_0(\rho) + f_2(\rho)\cos 2\varphi'$, where f_0 and f_2 are functions of ρ. The second term obviously cannot induce an electric field possessing a z' component on the symmetry axis of the tip-sample system, so we neglect it from now on. The cylindrically symmetric part of the field $\mathbf{E}^{\rm conv}(\boldsymbol{\rho})$ can be derived from a potential written as

$$\phi^c = \sqrt{2}\, a \sqrt{\cosh\beta - \cos\alpha} \sum_0^\infty T_n e^{-(n+1/2)\beta} P_n(\cos\alpha). \tag{B18}$$

The coefficients T_n in Eq. (B18) can be calculated with the aid of Eq. (B17). To this end we extract the cylindrically

symmetric part of $\hat{x}' \cdot \mathbf{E}_{\rm ind}^{\rm inc}$ by taking the average of its values on the x' and y' axis, respectively, and rewrite these expressions as sums of Legendre polynomials only. At the expense of introducing a more complicated prefactor this yields

$$\hat{x}' \cdot \mathbf{E}_{\rm ind}^{{\rm inc},x'(y')} = \sqrt{8} E^{\rm ext} \frac{\sqrt{1-\cos\alpha}}{1+\cos\alpha} \sum_0^\infty C_n^{x'(y')} P_n(\cos\alpha), \tag{B19}$$

where the superscript $x'(y')$ indicates whether the field is evaluated on the x' or y' axis. The coefficients $C_n^{x'}$ and $C_n^{y'}$ are given by rather lengthy expressions involving the A_n coefficients. It is also possible to rewrite $E_{z'}^{\rm c}$ resulting from the z' gradient of Eq. (B18) as a sum of Legendre polynomials preceded by the same prefactor as in Eq. (B19). From Eq. (B17) we then obtain the following equation system determining the T_n's:

$$v_n T_{n-2} + u_n T_n + w_n T_{n+2} = \frac{\epsilon_1(\omega)}{(\epsilon_S+1)^2} E^{\rm ext}(C_n^{x'} + C_n^{y'}), \tag{B20}$$

where

$$v_n = -\frac{1}{4}\frac{(n-1)n}{2n-1},$$

$$u_n = \frac{1}{4}\left(2n+1-\frac{(n+1)^2}{2n+3}-\frac{n^2}{2n-1}\right),$$

and

$$w_n = -\frac{1}{4}\frac{(n+1)(n+2)}{2n+3}. \tag{B21}$$

The final step amounts to solving for the enhancement of the z' component of the electric field between the tip and sample due to the presence of the tip. In fact, to obtain the final result for the degree of circular polarization, this calculation has to be done with two different driving forces. On one hand, using ϕ^c as a driving force we obtain E_z^s to be used in Eq. (10), if instead, as in Ref. 12, the potential corresponding to a reflected p wave is used to drive the tip-sample system, we obtain E_z^p to be used in Eq. (10). The two calculations can be done in parallel. We make an ansatz for the potentials induced due to the presence of the tip in the two cases

$$\phi_{\rm ind}^{c(p)} = \sqrt{2}\, a \sqrt{\cosh\beta - \cos\alpha} \sum_0^\infty F_n^{c(p)}(\beta) P_n(\cos\alpha), \tag{B22}$$

where the superscripts c and p, respectively, indicate that it is either the converted field or an incoming p wave that plays the role of driving force. In the sample ($\beta \leqslant 0$),

$$F_n^{c(p)}(\beta) = A_n^{c(p)} e^{(n+1/2)(\beta-\beta_0)} + B_n^{c(p)} e^{(n+1/2)(\beta+\beta_0)}, \tag{B23a}$$

in vacuum ($0 \leqslant \beta \leqslant \beta_0$)

$$F_n^{c(p)}(\beta) = A_n^{c(p)} e^{(n+1/2)(\beta-\beta_0)} + B_n^{c(p)} e^{-(n+1/2)(\beta-\beta_0)}, \tag{B23b}$$

and in the tip ($\beta \geqslant \beta_0$),

$$F_n^{c(p)}(\beta) = (A_n^{c(p)} + B_n^{c(p)}) e^{-(n+1/2)(\beta-\beta_0)}. \tag{B23c}$$

The external potential in the case of the converted field is given by Eq. (B18)

$$\phi^c = \sqrt{2}\, a \sqrt{\cosh\beta - \cos\alpha} \sum_0^\infty T_n e^{-(n+1/2)\beta} P_n(\cos\alpha),$$

whereas in the case of an incoming p wave it is

$$\phi_p^{\rm ext} = -\sin\theta \frac{2\epsilon_S p}{\epsilon_S p + p_t} E_p^{\rm inc} \sqrt{2}\, a \sqrt{\cosh\beta - \cos\alpha} \times \sum_0^\infty (2n+1) e^{-(n+1/2)\beta} P_n(\cos\alpha), \tag{B24}$$

where the first factor $\propto E_p^{\rm inc}$ is the resulting z' component of the **E** field just outside the sample surface as obtained from the Fresnel formulas.

Proceeding along the same lines as when deriving Eq. (B8), we first obtain

$$B_n^{c(p)} = -A_n^{c(p)} e^{-(2n+1)\beta_0} \chi_S \tag{B25}$$

and then the equation systems

$$U_n A_n^c + V_n A_{n-1}^c + W_n A_{n+1}^c = S_n^c \tag{B26}$$

and

$$U_n A_n^p + V_n A_{n-1}^p + W_n A_{n+1}^p = S_n^p \tag{B27}$$

determining the enhancement due to the presence of the tip of the converted field and the p polarized wave, respectively. The coefficients on the left hand side are the same in both cases,

$$U_n = (2n+1)\cosh\beta_0 (1 - \chi_S \chi_T e^{-(2n+1)\beta_0}) - \chi_T \sinh\beta_0 (1 - \chi_S e^{-(2n+1)\beta_0}), \tag{B28a}$$

$$V_n = -n(1 - \chi_S \chi_T e^{-(2n-1)\beta_0}), \tag{B28b}$$

$$W_n = -(n+1)(1 - \chi_S \chi_T e^{-(2n+3)\beta_0}). \tag{B28c}$$

The right hand side in Eq. (B26) is

$$S_n^c = \chi_T e^{-(n+1/2)\beta_0} \{[\sinh\beta_0 - (2n+1)\cosh\beta_0] T_n + n e^{\beta_0} T_{n-1} + (n+1) e^{-\beta_0} T_{n+1}\}, \tag{B29}$$

while for the case of an incident p wave we obtain

$$S_n^p = \sin\theta \frac{2\epsilon_S p}{\epsilon_S p + p_t} E_p^{\rm inc} \chi_T e^{-(n+1/2)\beta_0} \{(2n+1) \times [(2n+1)\cosh\beta_0 - \sinh\beta_0] - (2n^2 - n) e^{\beta_0} - (2n^2 + 5n + 3) e^{-\beta_0}\}. \tag{B30}$$

Once all the coefficients A_n^c and A_n^p have been determined using Eqs. (B25), (B26), and (B27), we can calculate the resulting electric fields on the symmetry axis as

$$E^{s}_{z'} = -\frac{\cosh\beta - \cos\alpha}{a}\left[\frac{\partial\phi^{c}}{\partial\beta} + \frac{\partial\phi^{c}_{\mathrm{ind}}}{\partial\beta}\right] \tag{B31}$$

and

$$E^{p}_{z'} = -\frac{\cosh\beta - \cos\alpha}{a}\left[\frac{\partial\phi^{\mathrm{ext}}_{p}}{\partial\beta} + \frac{\partial\phi^{p}_{\mathrm{ind}}}{\partial\beta}\right]. \tag{B32}$$

The degree of polarization of the emitted light is found from

$$\rho^{+} = \frac{S_3}{S_0} \approx -2\ \mathrm{Im}\left[\frac{E^{\mathrm{out}}_{s}}{E^{\mathrm{out}}_{p}}\right], \tag{B33}$$

so that using the reciprocity theorem, keeping in mind the sign change of ϵ_1 discussed earlier

$$\rho^{+} - \rho^{-} \approx 4\ \mathrm{Im}\left[\frac{E^{s}_{z'}}{E^{p}_{z'}}\right]. \tag{B34}$$

[1] R. L. Dubs, S. N. Dixit, and V. McKoy, Phys. Rev. Lett. **54**, 1249 (1985).

[2] C. F. Hague, J.-M. Mariot, P. Strange, P. J. Durham, and B. L. Gyorffy, Phys. Rev. B **48**, 3560 (1993).

[3] J. Bansmann, M. Getzlaff, C. Westphal, F. Fegel, and G. Schönhense, Surf. Sci. **269/270**, 622 (1992).

[4] A. L. Väzquez de Parga and S. F. Alvarado, Phys. Rev. Lett. **72**, 3726 (1994).

[5] N. Majlis, A. Levy Yeyati, F. Flores, and R. Monreal, Phys. Rev. B **52**, 12 505 (1995).

[6] Within the theory we will present here, the resolution would mainly be determined by the size of the electromagnetic cavity formed between the tip and sample. This leads to a resolution limit of the order of 50–100 Å .

[7] D. T. Pierce, A. Davies, J. A. Stroscio, and R. J. Celotta, Appl. Phys. A: Solids Surf. **66**, S403 (1998).

[8] A. L. Vázquez de Parga; and S. F. Alvarado, Europhys. Lett. **36**, 577 (1996).

[9] E. Anisimovas and P. Johansson, Phys. Rev. B **59**, 5126 (1999).

[10] S. F. Alvarado, in *Near Field Optics*, NATO Advanced Research Workshop on Near Field Optics, Arc-et-Senans, France, 1992, Ser. E, Vol. 242, edited by D. W. Pohl and D. Courjon (Kluwer, Dordrecht, 1993) p. 361.

[11] J. D. Jackson, *Classical Electrodynamics* (Wiley, New York, 1999).

[12] P. Johansson, R. Monreal, and P. Apell, Phys. Rev. B **42**, 9210 (1990); P. Johansson and R. Monreal, Z. Phys. B **69**, 284 (1991).

[13] J. A. Kong, *Theory of Electromagnetic Waves* (Wiley, New York, 1975), Sec. 7.2.

[14] R. Berndt, J. K. Gimzewski, and P. Johansson, Phys. Rev. Lett. **67**, 3796 (1991).

[15] V. A. Kosobukin, Phys. Solid State **39**, 488 (1997).

[16] P. Apell, Phys. Scr. **24**, 795 (1981).

[17] T. Takemori, M. Inoue, and K. Ohtaka, J. Phys. Soc. Jpn. **56**, 1587 (1987).

[18] J. Zak, E. R. Moog, C. Liu, and S. D. Bader, Phys. Rev. B **43**, 6423(E) (1992); **46**, 5883 (1991).

[19] H. Hulme, Proc. R. Soc. London **135**, 237 (1932).

[20] P. N. Argyres, Phys. Rev. **97**, 334 (1955).

[21] H. S. Bennet and E. A. Stern, Phys. Rev. **137**, A448 (1965).

[22] B. R. Cooper, Phys. Rev. **139**, A1504 (1965).

[23] T. Gasche, M. S. S. Brooks, and B. Johansson, Phys. Rev. B **53**, 296 (1996).

[24] A. Delin, O. Eriksson, B. Johansson, S. Auluck, and J. M. Wills (unpublished).

[25] G. S. Krinchik and V. A. Artem'ev, Zh. Éksp. Teor. Fiz. **53**, 1901 (1967) [Sov. Phys. JETP **26**, 1080 (1968)].

[26] D. Weller, G. R. Harp, R. F. C. Farrow, A. Cebollada, and J. Sticht, Phys. Rev. Lett. **72**, 2097 (1994).

[27] M. B. Stearns, in *Magnetic Properties of Metals*, Landolt-Börnstein, New Series, Group III, Vol. 19, Pt. a, edited by H. P. J. Wijn (Springer-Verlag, Berlin, 1986), pp. 113.

[28] The rapid behavior around $\hbar\omega = 3.6$ eV of the calculated results for a Ag tip in the sphere model is due to a dramatic decrease in the response to an incoming *p* polarized wave (cf. Ref. 12), which makes the degree of polarization extremely sensitive even to small variations, for example interpolation errors, of the dielectric functions. We wish to point out that these oscillations in $\rho^{+} - \rho^{-}$ can definitely not be observed experimentally, for the intensity of the emitted light for photon energies above 3.3–3.4 eV is extremely small.

[29] The dielectric tensor of Majlis *et al.*[5] is unphysical. The off-diagonal elements are constructed from the diagonal ones, an approach for which there is no theoretical justification, and the constructed tensor does not obey proper symmetry conditions for an absorbing medium. Furthermore the corresponding expression to our ρ_{ps} is not correct.

[30] E. R. Moog, S. D. Bader, and J. Zak, Appl. Phys. Lett. **56**, 2687 (1990).

[31] P. M. Morse and H. Feschbach, *Methods of Theoretical Physics* (McGraw-Hill, New York, 1953), Vol II, pp. 1298–1301.

[32] R. W. Rendell and D. J. Scalapino, Phys. Rev. B **24**, 3276 (1981).

[33] E. A. Stern, J. C. Mc Groddy, and W. E. Harte, Phys. Rev. **135**, A1306 (1964).